Available online at www.sciencedirect.com
SCIENCE DIRECT
Journal of Molecular Catalysis A: Chemical 250 (2006) 20–26
JOURNAL OF MOLECULAR CATALYSIS A: CHEMICAL
www.elsevier.com/locate/molcata

Chemistry and reactivity of dinuclear manganese oxamate complexes: Aerobic catechol oxidation catalyzed by high-valent bis(oxo)-bridged dimanganese(IV) complexes with a homologous series of binucleating 4,5-disubstituted-*o*-phenylenedioxamate ligands

Gonzalo Blay [a], Isabel Fernández [a], José R. Pedro [a,*], Rafael Ruiz-García [a], Tomás Temporal-Sánchez [a], Emilio Pardo [b], Francesc Lloret [b], M. Carmen Muñoz [c]

[a] *Departament de Química Orgànica, Universitat de València, 46100 Burjassot, València, Spain*
[b] *Departament de Química Inorgànica, Universitat de València, 46100 Burjassot, València, Spain*
[c] *Departamento de Física Aplicada, Universidad Politécnica de València, 46071 València, Spain*

Received 7 October 2005; accepted 5 January 2006
Available online 23 February 2006

Abstract

The high-valent bis(oxo)-bridged dimanganese(IV) complexes with the series of binucleating 4,5-X_2-*o*-phenylenebis(oxamate) ligands (opbaX_2; X = H, Cl, Me) (**1a**–**c**) have been synthesized and characterized structurally, spectroscopically and magnetically. Complexes **1a**–**c** possess unique $Mn_2(\mu\text{-}O)_2$ core structures with two *o*-phenylenediamidate type additional bridges which lead to exceptionally short Mn–Mn distances (2.63–2.65 Å) and fairly bent Mn–O–Mn angles (94.1°–94.6°). The cyclovoltammograms of **1a**–**c** in acetonitrile (25 °C, 0.1 M Bu_4NPF_6) show an irreversible one-electron oxidation peak at moderately high anodic potentials (E_{ap} = 0.50–0.85 V versus SCE), while no reductions are observed in the potential range studied (down to −2.0 V versus SCE). These dinuclear manganese oxamate complexes are excellent catalysts for the aerobic oxidation of 3,5-di-*tert*-butylcatechol to the corresponding *o*-quinone in acetonitrile at 25 °C. The order of increasing catecholase activity (k_{obs}) with the electron donor character of the ligand substituents as **1b** (X = Cl) < **1a** (X = H) < **1c** (X = Me) correlates with Hammett σ^+ values ($\rho = -0.95$). A mechanism involving initial activation of the catechol substrate by coordination to the dimetal center and subsequent oxidation to quinone by O_2 is proposed, which is consistent with the observed saturation kinetics.
© 2006 Elsevier B.V. All rights reserved.

Keywords: Catalysis; Catechols; Manganese; O–O bond activation; Oxidations; Redox properties

1. Introduction

Binuclear bis(oxo)-bridged metal active sites are an ubiquitous structural type in non-heme redox metalloenzymes [1–3]. Well-recognized examples include the higher oxidation state forms of manganese catalase (Cat) [1], iron methane monooxygenase (MMO) and iron ribonucleotide reductase (RR) [2]. For copper tyrosinase (Tyr) and copper catechol oxidase (CO) [3], there is a current debate on the occurrence of an equilibrium between the experimentally identified lower valent side-on peroxo-bridged form and the high-valent bis(oxo)-bridged form yet to be observed directly. On the basis of a variety of structural, spectroscopic, and reactivity studies on the enzymes themselves and their biomimetic inorganic models [4–6], it now seems to be agreed that the bis(μ-oxo)dimetal core in high oxidation states plays a key role in the understanding of the electronic properties and function of this class of enzymes. In an attempt to mimic the natural systems, an intensive research effort has been devoted to obtain synthetic low molecular weight analogues of these high-valent metalloenzyme intermediates, both structural and functional, often by reaction of lower valent precursors with dioxygen and its reduced derivatives [5]. Variation on the supporting ligands around the $M_2(\mu\text{-}O)_2$ core (M = Mn, Fe, Cu) and its influence in the reactivity of the resulting model complexes

* Corresponding author. Tel.: +34 963544329; fax: +34 963544328.
E-mail address: jose.r.pedro@uv.es (J.R. Pedro).

1381-1169/$ – see front matter © 2006 Elsevier B.V. All rights reserved.
doi:10.1016/j.molcata.2006.01.021

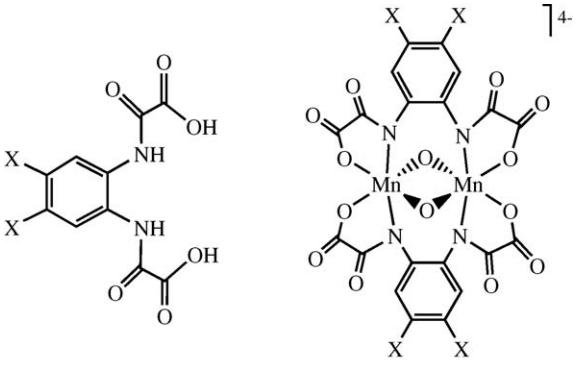

H_4opba: X = H
H_4opbaCl$_2$: X = Cl
H_4opbaMe$_2$: X = Me

1a: X = H
1b: X = Cl
1c: X = Me

Chart 1.

is key in elucidating the molecular basis of the catalytic mechanism for these biologically relevant non-heme dimetal enzymes [6].

We have recently reported on the stable bis(μ-oxo)dimanganese(IV) complex $(Ph_4P)_4[Mn_2O_2(opba)_2]\cdot 4H_2O$ (**1a**), which can be obtained by oxidation with H_2O_2 of the corresponding manganese(II) precursor, prepared in situ from a Mn^{2+} salt and the ligand *o*-phenylenebis(oxamic acid) (H_4opba) in basic solution under anaerobic conditions (Chart 1) [7]. The unprecedented binucleating bridging mode exhibited by the opba ligand, together with the presence of the strongly basic amidate donor groups, provide convenient access to modelize the active sites of non-heme binuclear enzymes in high oxidation states. In fact, this well-known class of aromatic dioxamate ligands with large electron donor ability commonly act in a mononucleating way toward middle (Mn, Fe) and late (Ni, Cu) 3d metal ions [8,9]. Based on this unexpected result, we decided to explore the aerobic oxidative catalytic properties of similar high-valent binuclear manganese oxamate complexes with H_4opba and related ligands differently substituted on the aromatic ring, either with electron acceptor substituents as in 4,5-dichloro-*o*-phenylenebis(oxamic acid) (H_4opbaCl$_2$) or with electron donor ones as in 4,5-dimethyl-*o*-phenylenebis(oxamic acid) (H_4opbaMe$_2$) (Chart 1). In the course of these studies, we synthesized the two new examples of stable bis(μ-oxo)dimanganese(IV) complexes $(Ph_4P)_4[Mn_2O_2(opbaCl_2)_2]\cdot 8H_2O$ (**1b**) and $(Ph_4P)_4[Mn_2O_2(opbaMe_2)_2]\cdot 16H_2O$ (**1c**) (Chart 1). Due to the potential relevance of a bis(oxo)dimetal core in the function of the copper enzymes CO and Tyr, we undertook a comparative kinetic study on the aerobic oxidation of catechols catalyzed by this series of manganese analogues **1a–c** in order to unravel possible differences in catecholase activity with change in the ligand electronic nature. Interestingly, the only two reported examples of catechol oxidation by related bis(μ-oxo)dicopper(III) complexes operate exclusively under stoichiometric conditions, leading to complex reduction and either quinone or semiquinone formation depending on the supporting ligand [10].

2. Experimental

2.1. Materials

All chemicals were of reagent grade quality, and they were purchased from commercial sources and used as received, except those for electrochemical measurements. The Bu_4NPF_6 salt was recrystallized twice from ethyl acetate–diethyl ether, dried at 80 °C under vacuum, and kept in an oven at 110 °C. Acetonitrile was purified by distillation from calcium hydride on to activated 3 Å molecular sieves and stored under argon. The diethylester derivatives of *o*-phenylenebis(oxamic acid) (H_2Et_2opba), 3,5-dichloro-*o*-phenylenebis(oxamic acid) (H_2Et_2opbaCl$_2$), and 3,5-dimethyl-*o*-phenylenebis(oxamic acid) (H_2Et_2opbaMe$_2$) were prepared by standard condensation techniques from the corresponding commercially available *o*-phenylenediamine derivatives and ethyloxalyl chloride in tetrahydrofuran as reported earlier [8,9].

2.2. Preparation

A 25% methanol solution of Me_4NOH (10.0 mL, 25.0 mmol) was added to a solution of the corresponding proligands H_2Et_2opbaX$_2$ (5.0 mmol) in methanol (50 mL) at room temperature under air. A methanol solution (25 mL) of $Mn(ClO_4)_2\cdot 6H_2O$ (1.79 g, 5 mmol) was then added dropwise under vigorous stirring. The reaction mixture was further stirred at room temperature for 30 min under air current to complete oxidation. The final dark-brown solution was filtered to eliminate the white solid NMe_4ClO_4, and then reduced to a final volume of 10 mL on a rotatory evaporator. The concentrated solution was treated successively with diethyl ether and acetone giving a dark-brown solid which was recuperated in water (50 mL). The resulting mixture was filtered to eliminate the rest of solid particles (mainly manganese dioxide). Ph_4PCl (3.75 g, 10 mmol) dissolved in the minimum amount of water was then added dropwise to the dark-brown solution. Slow evaporation of the filtered solution in air afforded well-shaped dark-brown crystals of **1a–c** after several weeks, which were filtered on paper and air-dried. Yields 35–50%. Anal. calc. for $C_{116}H_{96}Mn_2N_4O_{18}P_4$ (**1a**): C, 67.31; H, 4.64; N, 2.71. Found: C, 67.68; H, 4.60; N, 2.82. Anal. calc. for $C_{116}H_{100}Cl_4Mn_2N_4O_{22}P_4$ (**1b**): C, 61.16; H, 4.39; N, 2.46. Found: C, 61.23; H, 4.39; N, 2.57. Anal. calc. for $C_{120}H_{128}Mn_2N_4O_{30}P_4$ (**1c**): C, 61.54; H, 5.47; N, 2.39. Found: C, 61.31; H, 5.39; N, 2.51.

2.3. Crystal structure determination

Crystal data and structure refinement for **1c**: $C_{60}H_{64}MnN_2O_{15}P_2$, $M = 1170.01$, triclinic, space group *P*-1, $a = 14.1840$ (3) Å, $b = 14.3340$ (4) Å, $c = 16.8470$ (5) Å, $\alpha = 71.7140$ (10)°, $\beta = 67.6140$ (10)°, $\gamma = 68.7020$ (10)°, $V = 2888.97$ (13) Å^3, $Z = 2$, $T = 293$ (2) K, μ(Mo Kα) = 0.353 mm^{-1}, 12838 reflections measured, 8782 assumed as observed with $I > 2\sigma(I)$. Refinement on F^2 of 722 parameters with anisotropic thermal parameters for all non-hydrogen atoms

gave $R = 0.0796$, $R_w = 0.2140$, and GOF = 0.933 (observed data).

2.4. Physical techniques

Elemental analysis (C, H, N) were performed by the Microanalytical Service of the Universidad Autónoma de Madrid (Spain). IR spectra were recorded on a Perkin-Elmer 882 spectrophotometer as KBr pellets. UV–vis solution spectra were recorded on a Shimadzu UV-2401PC spectrophotometer. Variable-temperature (2.0–300 K) magnetic susceptibility measurements under an applied magnetic field of 1.0 T were carried out on powdered samples of **1a–c** with a SQUID magnetometer. Diamagnetic corrections to the susceptibility data were calculated from Pascal's constants, and they were also corrected for temperature-independent paramagnetism and the presence of paramagnetic impurities.

Cyclic voltammetry was performed using an EGG M273 PAR scanning potentiostat operating at a scan rate of 10–1000 mV s^{-1}. The electrochemical studies were carried out in acetonitrile using 0.1 M Bu_4NPF_6 as supporting electrolyte and 1.0 mM of complexes **1a–c**. The working electrode was a glassy carbon disk (0.32 cm^2) that was polished with 1.0 μm diamond powder, sonicated, washed with absolute ethanol and acetone, and air dried. The reference electrode was $AgClO_4$/Ag separated from the test solution by a salt bridge containing the solvent/supporting electrolyte, with platinum as auxiliary electrode. All experiments were performed in standard electrochemical cells at 25 °C under argon. The potential range investigated was between −2.00 and 1.80 V. The formal potentials were measured at a scan rate of 100 mV s^{-1} and were referred to the saturated calomel electrode (SCE), which was consistently measured as −0.26 V versus the $AgClO_4$/Ag electrode.

2.5. Reactivity studies

Kinetic measurements for the aerobic catechol oxidation reactions: the aerobic oxidation of the model substrate 3,5-di-*tert*-butyl catechol (H_2DTBC) catalyzed by **1a–c** was monitored by UV–vis spectroscopy by following the formation of the corresponding oxidation product 3,5-di-*tert*-butyl *o*-quinone (DTBQ) during the course of the reaction. The kinetic studies were carried out at $\lambda_{max} = 400$ nm ($\varepsilon = 1752 \pm 11$ M^{-1} cm^{-1}) which corresponds to the absorption maximum of DTBQ. The catalytic activity of **1a–c** was determined by the method of initial rates in the presence of a large initial excess of substrate (pseudo-first-order conditions). All experiments were carried out in a standard quartz cuvette (light-pathlength of 1 cm) in acetonitrile at 25 °C under aerobic conditions. In a first test series, varying amounts of a 10^{-3} M solution of the corresponding catalyst in acetonitrile (5.0–20.0 μL) were added to a 10^{-3} M solution of H_2DTBC in acetonitrile (2.0 mL). In a second test series, a 10^{-3} M solution of the corresponding complex in acetonitrile (20 μL) was added to solutions with varying concentrations of H_2DTBC (0.5–3.0 mM) in acetonitrile (2.0 mL).

Table 1
Selected physical data for **1a–c**

	1a	1b	1c
ν_{as}(CO)[a] (cm^{-1})	1672 (sh)	1672vs	1673vs
	1647vs	1649vs	1650vs
	1617vs	1619vs	1625 (sh)
ν_s(CO)[a] (cm^{-1})	1403s	1385s	1412s
	1306s	1294s	1312s
ν(MnO) (cm^{-1})	643m	638m	637m
λ_{max}(O → Mn CT)[b,c] (nm)	565 (1005)	575 (995)	575 (990)
	595 (940)	605 (990)	600 (920)
$-J$[d] (cm^{-1})	164	133	151
E_{ap} (V vs. SCE)[e]	0.68 (i)	0.85 (i)	0.50 (i)

[a] In KBr.
[b] In MeCN.
[c] The extinction coefficient (ε (M^{-1} cm^{-1})) values are given in parentheses.
[d] $H = -JS_1S_2$ ($S_1 = S_2 = 3/2$).
[e] In MeCN (25 °C, 0.1 M Bu_4NPF_6).

3. Results and discussion

3.1. Synthesis

Complexes **1a–c** were prepared by the straightforward reaction of $Mn(ClO_4)_2 \cdot 6H_2O$ and the corresponding proligands $H_2Et_2opbaX_2$ in basic methanol solution with excess Me_4NOH (1:5 ligand:base ratio) under air, and they were isolated as their tetraphenylphosphonium salts after methatesis with Ph_4PCl in water (Scheme 1). The chemical identity of **1a–c** has been confirmed by elemental analyses (see experimental), IR and UV–vis spectroscopies (Table 1). The similarities between

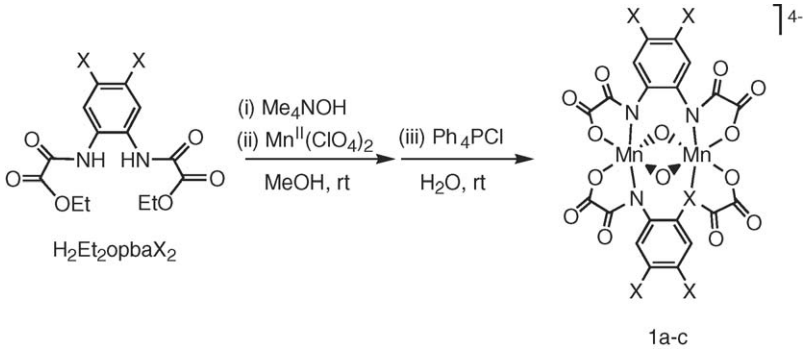

Scheme 1. Synthetic pathway to the manganese–opbaX$_2$ complexes.

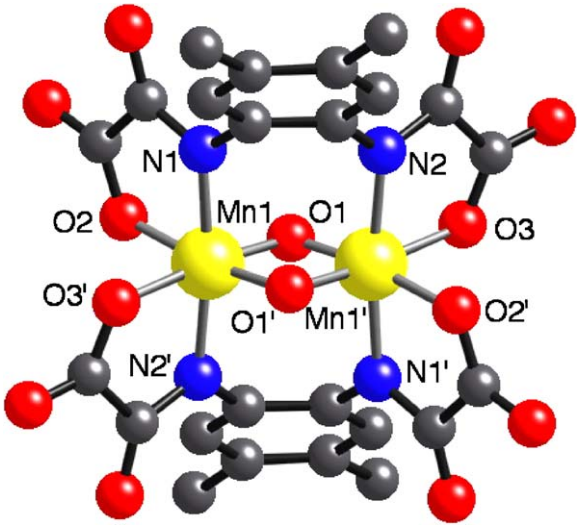

Fig. 1. Perspective view of the anionic dinuclear unit of **1c** with the atom-numbering scheme for the first coordination sphere of the metal atoms. Hydrogen atoms are omitted for clarity (symmetry code: $I = -x, -y, -z$).

the spectroscopic data indicate that the high-valent bis(μ-oxo)dimanganese(IV) description is the correct one for all three compounds and rule out the alternative lower valent bis(μ-hydroxo)dimanganese(III) formulation.

3.2. Structure

The structure of **1c** consists of dinuclear manganese(IV) complex anions $[Mn_2O_2(opbaMe_2)_2]^{4-}$ (Fig. 1), tetraphenylphosphonium cations, and crystallization water molecules. Selected bond distances and angles are listed in Table 2.

Table 2
Selected bond distances (Å) and angles (°) for **1c**[a,b]

Mn(1)–O(1)	1.800 (3)
Mn(1)–O(2)	1.977 (3)
Mn(1)–N(1)	1.982 (3)
Mn(1)–O(1^I)	1.803 (3)
Mn(1)–O(3^I)	1.972 (3)
Mn(1)–N(2^I)	1.985 (3)
O(1)–Mn(1)–O(1^I)	85.42 (12)
O(1)–Mn(1)–O(3^I)	95.72 (11)
O(1)–Mn(1)–N(2^I)	94.44 (12)
O(1^I)–Mn(1)–O(3^I)	173.13 (11)
O(1^I)–Mn(1)–N(2^I)	92.02 (13)
O(2)–Mn(1)–N(1)	81.93 (12)
O(3^I)–Mn(1)–N(1)	92.70 (12)
N(1)–Mn(1)–N(2^I)	172.57 (13)
O(1)–Mn(1)–O(2)	171.70 (11)
O(1)–Mn(1)–N(1)	90.28 (12)
O(1^I)–Mn(1)–O(2)	92.26 (12)
O(1^I)–Mn(1)–N(1)	94.08 (12)
O(2)–Mn(1)–O(3^I)	87.5 (12)
O(2)–Mn(1)–N(2^I)	93.60 (12)
O(3^I)–Mn(1)–N(2^I)	81.14 (12)
Mn(1)–O(1)–Mn(1^I)	94.58 (12)

[a] Estimated standard deviations are given in parentheses.
[b] Symmetry code: $I = -x, -y, -z$.

The 2.65 Å Mn–Mn and 2.44 Å O–O vectors in the planar Mn_2O_2 diamond core are comparable with those of **1a** (2.63 and 2.45 Å, respectively) [7]. The Mn–Mn distances are among the shortest ones yet reported for bis(oxo)-bridged dimanganese(IV) complexes (2.67–2.78 Å) [11]. As in complex **1a**, the binucleating bis(bidentate) $opbaMe_2$ ligand acts as a bridge between the two manganese atoms, which are then tightly tethered by the 4,5-dimethyl-*o*-phenylene linker between the apical *N*-amidate donor atoms. Within the $[Mn_2(\mu\text{-}O)_2(\mu\text{-}opbaMe_2)_2]^{4-}$ bridging unit, the average Mn–O and Mn–N bond lengths of 1.80 and 1.98 Å, respectively, are almost identical to those in **1a** (1.80 and 2.00 Å, respectively), while the Mn–O–Mn angle of 94.6° is slightly less bent (94.1°) [7]. Two basal *O*-carboxylate donor atoms from the oxamate groups complete the octahedral coordination sphere of each Mn atom, with an average Mn–O bond length of 1.97 Å which is identical to that in **1a**. Overall, this carboxylate-rich environment is reminiscent of that found in the active sites of non-heme dimanganese and diiron enzymes [1,2], but contrasts with the all-imidazole terminal ligation of dicopper enzymes [3].

3.3. Magnetic properties

The variable-temperature magnetic susceptibility data of **1a–c** in the form of the χ_M versus T plot (χ_M being the molar magnetic susceptibility and T the temperature) are typical of antiferromagnetically coupled Mn_2^{IV} pairs with a diamagnetic singlet ($S = 0$) ground state (Fig. 2). Upon cooling from room temperature, χ_M decreases continuously and vanishes at 25 K. The least-squares fits of the experimental data through the appropriate spin Hamiltonian $[H = -JS_1S_2 + g\beta(S_1 + S_2)B; S_1 = S_2 = 3/2]$ gave exchange coupling constant ($-J$) values in the narrow range 133–164 cm^{-1} (Table 1), with a common isotropic Zeeman factor (g) value of 2.0 (solid lines in Fig. 2). The $-J$ values for **1a–c** are among the smallest ones yet reported for strongly coupled bis(oxo)-bridged dimanganese(IV) complexes ($-J = 156$–$376\ cm^{-1}$) [11]. According to a recent magneto-

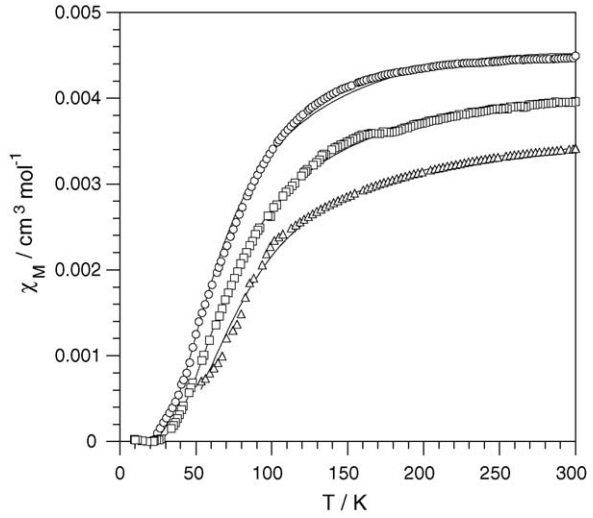

Fig. 2. Temperature dependence of χ_M for **1a** (△), **1b** (◯), and **1c** (□). Solid lines correspond to the best fits.

structural correlation for bis(μ-oxo)dimanganese(IV) compounds [11], the moderately strong antiferromagnetic coupling in **1a–c** reflects the fairly acute Mn–O–Mn angle which is likely associated with the presence of the two *o*-phenylenediamidate type supporting bridges.

3.4. Redox properties

The cyclic voltammetry data of **1a–c** in acetonitrile at 25 °C exhibit a common pattern. The cyclovoltammograms show an irreversible oxidation peak at moderately high anodic potentials (E_{ap}) in the range 0.50–0.85 V versus SCE (Fig. 3). The large variation in the E_{ap} values along this series suggests a primarily ligand-centered redox process. When compared to **1a** (X = H), they increase by over 170 mV for **1b** (X = Cl), while decrease by 180 mV for **1c** (X = Me) (Table 1), as expected for the electron acceptor and electron donor nature of the ligand substituents, respectively. Importantly, no reductions are observed in the potential range studied (down to −2.0 V versus SCE). This indicates that mixed-valent Mn(III, IV)$_2$O$_2$ and lower valent Mn(III, III)$_2$O$_2$ species are not available for this series of high-valent bis(μ-oxo)dimanganese(IV) oxamate complexes, which then are poor oxidizing agents owing to the large σ-donor effect of the amidate donor groups.

3.5. Reactivity properties

The catecholase activity of **1a–c** has been examined in acetonitrile at 25 °C under aerobic conditions. Complexes **1a–c** shown moderate to high catalytic activities toward the aerobic oxidation of the model substrate 3,5-di-*tert*-butyl catechol (H_2DTBC) to the corresponding *o*-quinone (DTBQ) as sole oxidation product. For instance, following a short induction period of a few minutes, complete conversion is achieved after 0.5 h for **1a** (TON = 100) (Fig. 4). To our knowledge, there are only

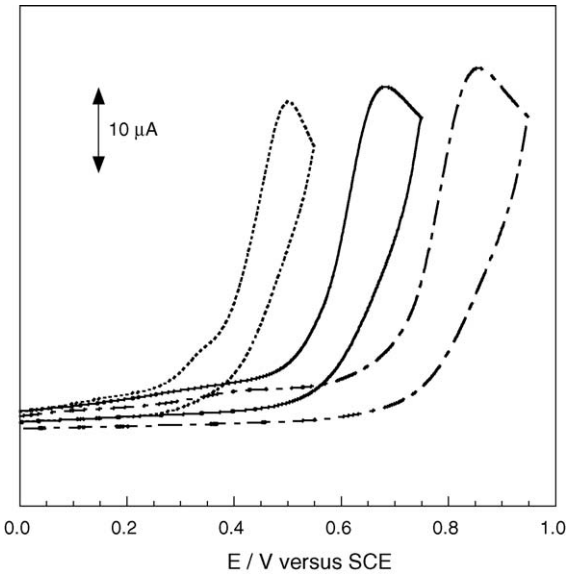

Fig. 3. Cyclovoltammograms of **1a** (—), **1b** (–·–), and **1c** (···) in MeCN at 25 °C and at scan rate of 100 mV s^{-1}.

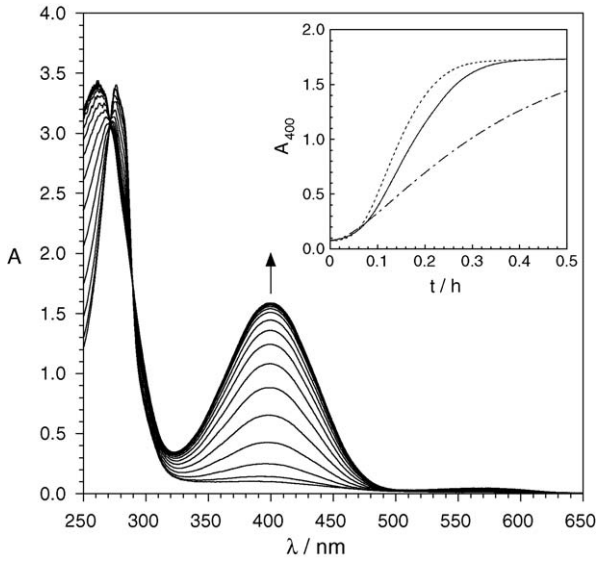

Fig. 4. UV–vis spectral changes for the aerobic oxidation of H_2DTBC catalyzed by **1a** in MeCN at 25 °C ([H_2DTBC] = 10^{-3} M and [**1a**] = 10^{-5} M). The inset shows the time course of the absorbance at 400 nm (A_{400}) for the aerobic oxidation of H_2DTBC catalyzed by **1a** (—), **1b** (–·–), and **1c** (···) in MeCN at 25 °C ([H_2DTBC] = 10^{-3} M and [1] = 10^{-5} M).

two reports of similar manganese catecholase analogues based on the mixed-valent bis(μ-oxo) dimanganese(III, IV) complex [Mn_2O_2(cyclam)$_2$](ClO$_4$)$_3$ (cyclam = 1,4,8,11-tetraazacyclotetradecane) [12] and the lower-valent bis(μ-oxo) dimanganese(III) complex [Mn_2O_2(tpa)$_2$](BPh$_4$)$_2$ [tpa = tris(pyridin-2-ylmethyl)amine] [13].

The kinetics of the catecholase model reactions under pseudo-first-order conditions of substrate revealed a linear dependence of the initial rate (v_0) on the catalyst concentration (Fig. 5). This suggests cooperative action of the two metal centers for the two-electron oxidation of the catechol substrate molecule. The calculated pseudo-first-order rate constant (k_{obs}) values of 238–699 h^{-1} for **1a–c** at [H_2DTBC] = 10^{-3} M allow to obtain corresponding second-order rate constant (k_s) values

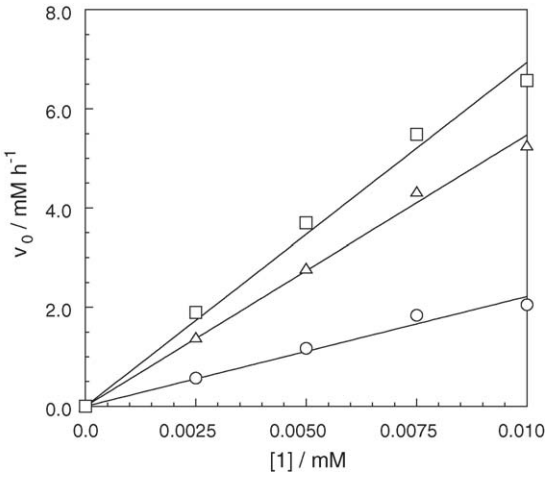

Fig. 5. Catalyst concentration dependence on the initial rate (v_0) of aerobic oxidation of H_2DTBC catalyzed by **1a** (△), **1b** (◯), and **1c** (□) in MeCN at 25 °C ([H_2DTBC] = 10^{-3} M). Solid lines correspond to the best fits.

Table 3
Selected kinetic data for the aerobic oxidation of H_2DTBC catalyzed by **1a–c**[a]

	1a	1b	1c
k_{obs}[b] (h^{-1})	547 ± 11	238 ± 23	699 ± 27
$k_s \times 10^{-5}$[c] ($M^{-1}\,h^{-1}$)	5.47 ± 0.11	2.38 ± 0.23	6.99 ± 0.27
$K_M \times 10^3$[d] (M)	2.4 ± 0.4	3.1 ± 0.6	2.0 ± 0.4
$v_{max} \times 10^3$[d] ($M\,h^{-1}$)	15.6 ± 1.8	9.4 ± 1.4	16.2 ± 2.2
k_{cat}[e] (h^{-1})	1560 ± 180	940 ± 140	1620 ± 220

[a] In MeCN at 25 °C.
[b] Determined from a linear plot (v_0 vs. [**1**]).
[c] $k_{obs} = k_s[H_2DTBC]$ ($[H_2DTBC] = 10^{-3}$ M).
[d] Determined from a Lineweaver–Burke plot ($1/v_0$ vs. $1/[H_2DTBC]$).
[e] $v_{max} = k_{cat}[\mathbf{1}]$ ($[\mathbf{1}] = 10^{-5}$ M).

of 2.38×10^5–$6.99 \times 10^5\ M^{-1}\,h^{-1}$ (Table 3). These values are rather high compared with that of $[Mn_2O_2(cyclam)_2](ClO_4)_3$ which catalytically oxidize catechol to *o*-quinone by a simple outer-sphere redox mechanism ($k_s = 8.32 \times 10^3\ M^{-1}\,h^{-1}$ in water at pH 7.0, 30 °C) [12]. The variation in the k_{obs} values along the present series does not agree, however, with an electron transfer role for the complex in the metal-catalyzed catechol oxidation, in accordance with the aforementioned redox properties. Thus, complex **1c** (X = Me) is about 1.3 times faster than **1a** (X = H), while **1b** (X = Cl) is 2.3 times slower (Table 2), which is exactly the reverse trend in the expected oxidizing power.

On the other hand, saturation kinetics of the catecholase model reactions was observed for the initial rate dependence on the substrate concentration (Fig. 6). This indicates that an intermediate complex-substrate adduct forms in a preequilibrium process and that the irreversible substrate oxidation is the rate-determining step of the catalytic cycle. A Michaelis–Menten analysis of the experimental data yielded equilibrium constant (K_M) values of 2.0×10^{-3}–3.1×10^{-3} M and rate constant (k_{cat}) values of 940–1620 h^{-1} (Table 3) (solid lines in Fig. 6). These values are higher than those reported for $[Mn_2O_2(tpa)_2](BPh_4)_2$ which catalytically oxidize catechol to *o*-quinone by a more complex inner-sphere redox mechanism under the same reaction conditions ($K_M = 0.5 \times 10^{-3}$ M and $k_{cat} = 336\ h^{-1}$ in acetonitrile, 25 °C) [13]. The order of increasing K_M values as **1c** (X = Me) < **1a** (X = H) < **1b** (X = Cl) correlates with the electron acceptor character of the ligand substituents. More electron-withdrawing substituents should enhance the coordinating capacity (Lewis acidity) of the metal centers thus favoring dimetal-catechol association. Contrarily, the order of increasing k_{cat} values as **1b** (X = Cl) < **1a** (X = H) < **1c** (X = Me) agrees with the first estimation based on the k_{obs} values and correlates with the electron donor character of the ligand substituents. More electron-releasing substituents should attenuate the charge donation from the coordinated catechol to the metal centers in the putative dimetal-catechol intermediate, thereby making the substrate more prone to oxidation by O_2. Hammett plots of $\log(k_{cat})$ and $\log(k_{obs})$ versus σ^+ values gave negative ρ values of −0.50 and −0.95, respectively, while that of $\log(K_M)$ gave a positive ρ value of +0.35 (Fig. 7). The small negative ρ value of −0.50 for $\log(k_{cat})$ supports a rate-controlling electrophilic attack at the aromatic π-system of the catechol with slight build-up of positive charge in the polar transition state.

A mechanism for the aerobic catechol oxidation catalyzed by complexes **1a–c** involving initial activation of the catechol substrate by coordination to the dimetal center and subsequent oxidation to quinone by O_2 is proposed, which is consistent with the observed saturation kinetics (Scheme 2). More likely, substrate binding occurs after doubly deprotonation of the substrate by a bridging oxo group with release of a water molecule, leading to a bridging catecholate as proposed for the catecholase catalytic cycle of the enzymes Tyr and CO and their dicopper model systems [3,14]. In the present dimanganese catecholase model system, however, there is no intramolecular two-electron transfer to produce the *o*-quinone product and regenerate the lower valent dimetal center. Instead, the catecholase activity of **1a–c** rests on the Lewis acid character of the metal ions, which activate the bound catecholate for the two-electron oxidation to *o*-quinone by dioxygen.

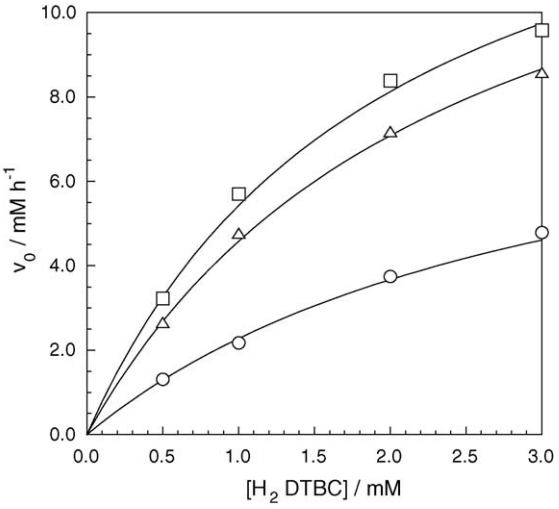

Fig. 6. Substrate concentration dependence on the initial rate (v_0) of aerobic oxidation of H_2DTBC catalyzed by **1a** (△), **1b** (◯), and **2c** (□) in MeCN at 25 °C ($[1] = 10^{-5}$ M). Solid lines correspond to the best fits.

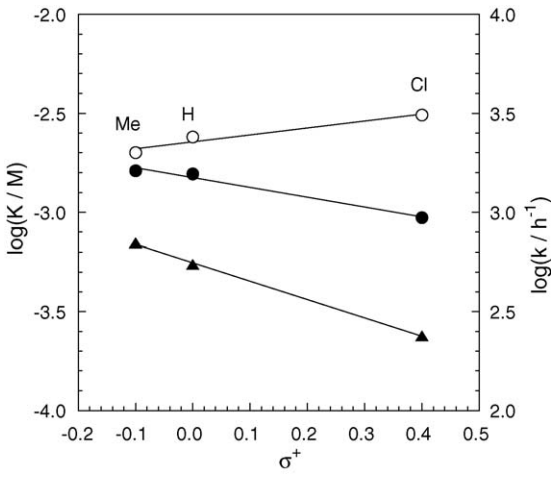

Fig. 7. Hammett plots of K_M (◯), k_{cat} (●), and k_{obs} (▲) for the aerobic oxidation of H_2DTBC catalyzed by **1a** (X = H), **1b** (X = Cl), and **1c** (X = Me) in MeCN at 25 °C. Solid lines correspond to the best fits.

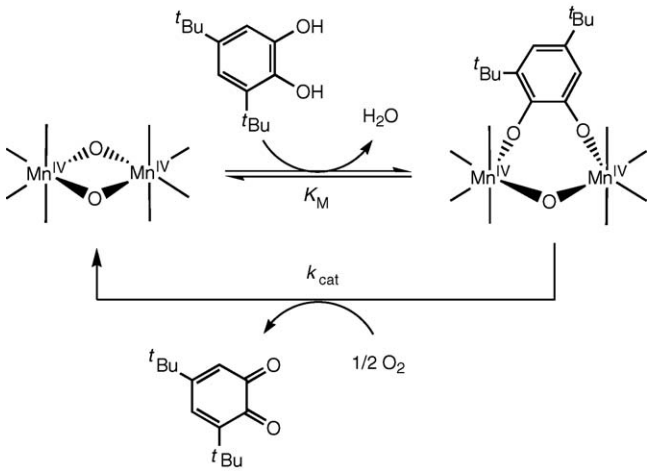

Scheme 2. Proposed mechanistic pathway for the aerobic catechol oxidation catalyzed by the manganese–opbaX_2 complexes.

4. Conclusions

A novel series of stable high-valent bis(oxo)-bridged dimanganese(IV) complexes with the binucleating bridging oxamate ligands opbaX_2 (X = H, Cl, Me) has been developed as efficient catechol oxidase models. A balanced ligand design allows to tune the catalytic activity along this series by varying the electronic nature of the X groups. Some aspects of the reaction mechanism are reminiscent of those proposed for the catecholase catalytic cycle of the enzymes Tyr and CO. Yet, it is substantially different in nature due more likely to the distinct redox and reactivity profiles of the high-valent bis(μ-oxo)dicopper sites and their bis(μ-oxo)dimanganese analogues. Further mechanistic studies are in progress to determine the exact chemical nature of the intermediate species involved in this bioinspired manganese-based catechol oxidase model system.

5. Supplementary material

Crystallographic data (excluding structure factors) for **1c** have been deposited with the Cambridge Crystallographic Data Centre, CCDC No. 284209. Copies of the data may be obtained free of charge on application to The Director, CCDC, 12 Union Road, Cambridge CB2 1EZ, UK (Fax: +44 1223 336 033; e-mail: mailto:deposit@ccdc.cam.ac.uk or www: http://www.ccdc.cam.ac.uk/).

Acknowledgements

This work was supported by the Ministerio de Ciencia y Tecnología (Spain) (Project BQU2001-3017) and the Ramón y Cajal program. Further support from the Generalitat Valenciana (Spain) (Project CTIDIA2002-131 and AVCYT Grupos 03/168) is also acknowledged. E. P. thanks the Ministerio de Educación, Cultura y Deporte (Spain) for a grant.

References

[1] G.C. Dismukes, Chem. Rev. 96 (1996) 2909.
[2] (a) B.J. Wallar, J.D. Lipscomb, Chem. Rev. 96 (1996) 2625;
(b) B.M. Sjöberg, Struct. Bonding (Berl.) 88 (1997) 139;
(c) M. Merkx, D.A. Kopp, M.H. Sazinsky, J.L. Blazyk, J. Müller, S.J. Lippard, Angew. Chem. Int. Ed. 40 (2001) 2782.
[3] (a) E.I. Solomon, U.M. Sundaram, T.E. Machonkin, Chem. Rev. 96 (1996) 2563;
(b) E.I. Solomon, P. Chen, M. Metz, S.K. Lee, A.E. Palmer, Angew. Chem. Int. Ed. 40 (2001) 4570;
(c) C. Gerdemann, C. Eicken, B. Krebs, Acc. Chem. Res. 35 (2002) 183.
[4] (a) A.J. Wu, J.E. Penner-Hahn, V.L. Pecoraro, Chem. Rev. 104 (2004) 903;
(b) E.Y. Tshuva, S.J. Lippard, Chem. Rev. 104 (2004) 987;
(c) L.M. Mirica, X. Ottenwaelder, T.D.P. Stack, Chem. Rev. 104 (2004) 1013;
(d) E.A. Lewis, W.B. Tolman, Chem. Rev. 104 (2004) 1047.
[5] (a) V.L. Pecoraro, M.J. Baldwin, A. Gelasco, Chem. Rev. 94 (1994) 807;
(b) L. Que Jr., Y. Dong, Acc. Chem. Res. 29 (1996) 190;
(c) W.B. Tolman, Acc. Chem. Res. 30 (1997) 227.
[6] (a) J.B. Vincent, G. Christou, Adv. Inorg. Chem. 33 (1989) 197;
(b) L. Que Jr., W.B. Tolman, Angew. Chem. Int. Ed. 41 (2002) 1114.
[7] R. Ruiz, A. Aukauloo, Y. Journaux, I. Fernández, J.R. Pedro, A.L. Roselló, B. Cervera, I. Castro, M.C. Muñoz, Chem. Commun. (1998) 989.
[8] M. Tettouhi, L. Ouahab, A. Boukhari, O. Cador, C. Mathoniere, O. Kahn, Inorg. Chem. 35 (1996) 4932.
[9] (a) R. Ruiz, M. Traianidis, A. Aukauloo, Y. Journaux, I. Fernández, J.R. Pedro, B. Cervera, I. Castro, M.C. Muñoz, Chem. Commun. (1997) 2283;
(b) B. Cervera, J.L. Sanz, M.J. Ibañez, G. Vila, F. Lloret, M. Julve, R. Ruiz, X. Ottenwaelder, A. Aukauloo, S. Poussereau, Y. Journaux, M.C. Muñoz, J. Chem. Soc., Dalton Trans. (1998) 781;
(c) G. Blay, I. Fernández, T. Giménez, J.R. Pedro, R. Ruiz, E. Pardo, F. Lloret, M.C. Muñoz, Chem. Commun. (2001) 2102;
(d) X. Ottenwaelder, R. Ruiz-García, G. Blondin, R. Carrasco, J. Cano, D. Lexa, Y. Journaux, A. Aukauloo, Chem. Commun. (2004) 504.
[10] (a) V. Mahadevan, J.L. DuBois, B. Hedman, K.O. Hodgson, T.D.P. Stack, J. Am. Chem. Soc. 121 (1999) 5583;
(b) L.M. Berreau, S. Mahapatra, J.A. Halfen, R.P. Houser, V.J. Young Jr., W.B. Tolman, Angew. Chem. Int. Ed. 38 (1999) 207.
[11] N.A. Law, J.W. Kampf, V.L. Pecoraro, Inorg. Chim. Acta 297 (2000) 252.
[12] N. Shaikh, M. Ali, P. Banerjee, Inorg. Chim. Acta 339 (2002) 341.
[13] Y. Hitomi, A. Ando, H. Matsui, T. Ito, T. Tanaka, S. Ogo, T. Funabiki, Inorg. Chem. 44 (2005) 3473.
[14] (a) K.D. Karlin, Y. Gultneh, T. Nicholson, J. Zubieta, Inorg. Chem. 24 (1985) 3725;
(b) H. Börzel, P. Comba, H. Pritzkow, Chem. Commun. (2001) 97;
(c) S. Torrelli, C. Belle, S. Hamman, J.L. Pierre, E. Saint-Aman, Inorg. Chem. 41 (2002) 3983.